Effect of surfactant on bubble collisions on a free surface

Shiyan Wang, Tianqi Guo, Sadegh Dabiri, Pavlos P. Vlachos, and Arezoo M. Ardekani

Phys. Rev. Fluids **2**, 043601 — Published 18 April 2017

DOI: 10.1103/PhysRevFluids.2.043601

Effect of surfactant on bubble collisions on a free surface

Shiyan Wang,[1] Tianqi Guo,[1] Sadegh Dabiri,[1,2] Pavlos P. Vlachos,[1] and Arezoo M. Ardekani[1]

[1]*School of Mechanical Engineering, Purdue University, West Lafayette, IN 47907, USA*

[2]*School of Agricultural & Biological Engineering, Purdue University, West Lafayette, IN 47907, USA*

(Dated: March 24, 2017)

Abstract

We report on the coefficient of restitution of bubble collision on a free surface in the presence of surfactants. In pure fluids, the collision process is well described by a competition between thin film drainage and interfacial tension. When surfactants are introduced in the pure water, they generate Marangoni stresses on both the bubble interface and free surface, which provides an additional mechanism affecting the collision process. We investigate this mechanism for the bubble collision process in surfactant solutions through a combination of experimental and numerical approaches, with results showing a reduced rebound velocity during the collision process in surfactant solutions compared with that in the pure water. Furthermore, by varying both bubble size and surfactant concentration, our experiments show that bubbles experience elastic, partially inelastic and perfectly inelastic collisions. We identify the Langmuir number, the ratio between absorption and desorption rates, as the fundamental parameter that quantifies the Marangoni effect on the collision process. The effect of Marangoni stress on the bubble's coefficient of restitution is non-monotonic, where the coefficient of restitution first decreases with Langmuir number, and then increases.

I. INTRODUCTION

Surfactants are known to effectively reduce the rate at which bubbles rise in pure fluids [1, 2]. The first physical explanation of this phenomenon is given by Frumkin & Levich [3]. For a translating bubble, surfactants on the bubble interface are adsorbed from the bulk solution, generating Marangoni stresses that reduce interfacial mobility and increase the drag acting on the rising bubble. To date, several papers have discussed the effect of surfactants on bubble's drag coefficient [4, 5], its lift force under shear flow [6], and its steady-state velocity [1, 7]. For a bubble rising rectilinearly in a surfactant solution, the reduced steady-state velocity can be simulated using a stagnant cap model, which assumes a no-slip velocity within the cap region and zero shear condition at the remaining portion of the bubble interface [1]. Cuenot *et al.* [4] solved the full Navier-Stokes equations coupled with the bulk and interfacial surfactant concentration equations. Their numerical study confirmed the validity of the stagnant-cap model, and furthermore, they studied the transient evolution of the flow over a spherical bubble in surfactant solutions.

Large bubbles [8] and multiple bubble interactions [2] have been observed in practical systems, where the effects of non-spherical shape and dynamic interfacial interactions need to be considered. For an isolated large air bubble (diameter larger than 2 mm) in quiescent water, surfactants changed its path instability [8]. Recent numerical simulations [9–11] have revealed the significance of surfactant affecting the transient behavior of a non-spherical bubble. In a bubbly flow, surfactants could change the flow structure through altering bubble-bubble interactions and inhibiting the coalescence of small bubbles [2].

Studies on interactions between air bubbles and free surface are important for both environmental and industrial applications. The interactions may lead to the coalescence of gas bubbles in mass transfer equipments such as bubble columns, decreasing overall interfacial area [12]. Despite decades of research studying the collision process in pure liquids [13–17], the relevant bubble dynamics in surfactant solutions are poorly understood. In this work, we conduct experimental studies, aided by the numerical simulations, to examine the effect of surfactant on rising bubbles colliding on a free surface. Section 2 describes the experimental setup. We report the mathematical models and numerical implementations for multiphase flows in surfactant solutions in section 3. In section 4, we first compare the bubble dynamics in both pure water and surfactant solutions. Subsequently, we examine the effect of surfac-

tants on both the drag acting on the rising bubbles and their collision processes. Finally, we conclude with our findings of this study in section 5.

II. EXPERIMENTAL SECTION

The experimental setup is shown in Figure 1(a). Air bubbles were generated by either a borosilicate glass capillary or a stainless steel needle that was installed at the center of the 3D-printed base and was connected with a precision syringe pump (PHD Ultra) from Harvard Apparatus. Generated bubble radii ranged from 0.44 mm to 0.84 mm. The test container (size: 1 in $\times$ 1 in $\times$ 4 in) was made of borosilicate glass. Before conducting each experiment, we eliminated container's contaminations using ultrasonic bath with ultra-pure water. The ultra-pure water was supplied by purification system (Barnstead MicroPure UF/UV, Thermo Scientific). Its electric resistivity was 18.2 $M\Omega \cdot cm$ (18.18 $M\Omega \cdot cm$ for ultra-pure water [18]). The conductivity and total organic carbon in the water were 0.055 $\mu S \cdot cm^{-1}$ and 5 p.p.b., respectively. We chose 1-pentanol as our surfactant model due to its well-known kinematics of dynamic adsorption [19, 20]. The concentration of 1-pentanol solution ranged from 0 to 200 mM (0 % to 8 % of critical micellar concentration (CMC)). The surface tension value between air and 1-pentanol solution was measured using a pendant droplet tensiometer (Ramé-Hart 500), and was found in good agreement with the Szyszkowski equation [21] (see the Appendix). A CMOS camera (Phantom Miro M340, Vision Research) mounted on a micro-stage recorded images at 1600 $\sim$ 3000 frames/s. The images were pre-processed by taking the inverse intensity, and a subsequent local minimum background subtraction to eliminate background noise. The bubble center was determined by calculating the geometric center of the generated binary image with a pre-selected intensity threshold. The instantaneous bubble velocity was obtained by taking the central difference of the bubble's vertical position with respect to time. The temporal evolution of the translational velocity of a 0.66 mm bubble in both pure water (black solid triangles) and 5 mM 1-pentanol solution (red solid circles) is shown in Figure 2(a). We should note that there is a period during which the bubble collides on and is in contact with the free surface, and position and centroid measurements contain large error. Consequently, measurement uncertainties for bubble centroid are large. Therefore, we exclude all experimental data for this period in Figure 2.

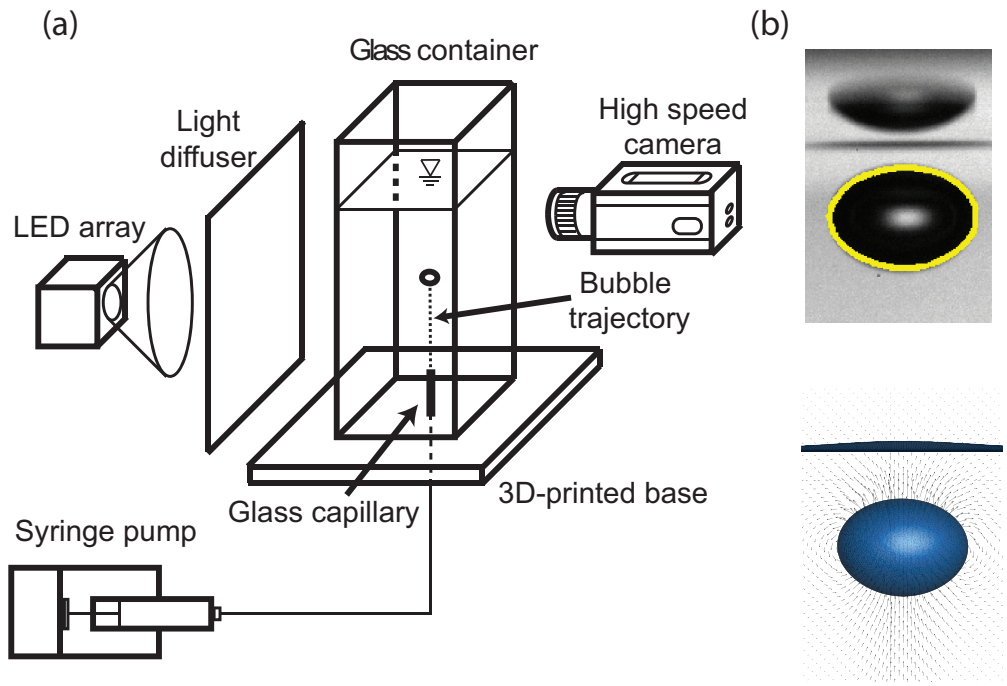

FIG. 1. (Color online)(a) The schematic diagram of the experimental setup. (b) A direct comparison of a raw image of an ascending bubble ($R = 0.66\ mm$) using experiments and 3D numerical simulation in pure water. The vectors in 3D numerical simulation indicate flow velocity.

III. MATHEMATICAL MODEL AND NUMERICAL IMPLEMENTATION

A. Mathematical model

In this section, we describe the mathematical model for both rising motion of gas bubbles and their collisions on a free surface. Both gas and liquid phases are homogenous fluids (see Figure 1(b)). The equations of motion for viscous, incompressible fluids in the entire computational domain are

$$\nabla \cdot \mathbf{u} = 0, \tag{1}$$

$$\rho \frac{D\mathbf{u}}{Dt} = -\nabla p + \mu \nabla^2 \mathbf{u} + \rho \mathbf{g} + \mathbf{f}, \tag{2}$$

where t is time, $\mathbf{u}$ is the flow velocity, p is the hydrodynamic pressure, $\mathbf{g}$ is the gravitational acceleration, μ is the dynamic viscosity of the fluid, and ρ is the fluid density. $D(\cdot)/Dt$ is the material derivative. Since fluid properties remain constant within each phase, $\frac{D\rho}{Dt} = 0$ and $\frac{D\mu}{Dt} = 0$. The density ρ and viscosity μ can be written as $\rho = \rho_i + \phi(\rho_o - \rho_i)$ and $\mu = \mu_i + \phi(\mu_o - \mu_i)$, where subscripts i and o refer to gas phase and liquid phase, respectively;

the indicator function ϕ separates two phases with $\phi = 1$ for the bulk liquid and $\phi = 0$ for the gas phase. The surface tension force $\mathbf{f}$ in the momentum equation, Eq. (2), acts on the interfaces (free surface and bubble interface),

$$\mathbf{f} = 2 \int_A \sigma \kappa \mathbf{n} \delta \left(\mathbf{x} - \mathbf{x}_f \right) dA, \tag{3}$$

where σ is the surface tension coefficient; dA is the surface differential element; κ is the mean curvature of the interface; $\mathbf{n}$ is the unit vector normal to the interface. The interface can be described by a collection of distributed points $\mathbf{x}_f$. Three dimensional delta function δ is used to calculate interfacial force, which is only nonzero on the interface.

Surfactants are soluble, and mass transfer occurs between the bulk fluid and the interface. We write the convection-diffusion equations for both bulk concentration C and interfacial concentration Γ, respectively,

$$\frac{\partial C}{\partial t} + \nabla \cdot (\mathbf{u} C) = \nabla \cdot (D_c \nabla C) + \dot{S}_c, \tag{4}$$

$$\frac{\partial \Gamma}{\partial t} + \nabla_s \cdot (\Gamma \mathbf{U}_s) = D_s \nabla_s^2 \Gamma + \dot{S}_\Gamma, \tag{5}$$

where $\mathbf{U}_s$ is the tangential velocity on the interface; the surfactant is impermeable to gas phase, therefore $D_c = D_o \phi$; D_o is the molecular diffusion coefficient of surfactant in the bulk liquid; $\nabla_s = \nabla - \mathbf{n} (\mathbf{n} \cdot \nabla)$ is the surface gradient defined at the interface; D_s is the interfacial diffusion coefficient of the surfactant. The dynamic adsorption of surfactant on the interface is given by

$$\dot{S}_\Gamma = k_a C_s \left(1 - \Gamma / \Gamma_\infty \right) - k_d \Gamma, \tag{6}$$

and this source term is related to the bulk concentration via the following relationship

$$\dot{S}_\Gamma = -D_c \left(\mathbf{n} \cdot \nabla C |_{C = C_s} \right), \tag{7}$$

where k_a and k_d are the adsorption and desorption rate constants, respectively; C_s is the surfactant bulk concentration evaluated adjacent to the interface; Γ_∞ is the maximum interfacial surfactant concentration. The value of surface tension coefficient is directly affected by the interfacial surfactant concentration Γ, and it is written as $\sigma / \sigma_0 = 1 + \beta \ln (1 - \Gamma / \Gamma_\infty)$, where $\beta = \mathscr{R} T \Gamma_\infty / \sigma_0$ characterizes the sensitivity of surface tension σ to interfacial surfactant concentration Γ, $\mathscr{R}$ is the ideal gas constant and σ_0 is the surface tension of a clean interface at room temperature T. For our experiments, the room temperature is kept at

21°C, and σ_0 is about 72.2 mN/m which is consistent with previous literature [19, 20]. Therefore, for 1-pentanol solution, $\beta = 0.20$. The time scale [8] for achieving the equilibrium interfacial surfactant concentration can be estimated as $\tau_e \sim (k_a C_\infty/\Gamma_\infty + k_d)^{-1}$, where C_∞ is the initial surfactant bulk concentration. Therefore, surfactant solution with a high bulk concentration quickly reaches equilibrium. For 1-pentanol solution, Γ_∞, k_a, and k_d are invariant under different bulk concentrations [19, 20]: $\Gamma_\infty = 5.90 \times 10^{-10}\ mol \cdot cm^{-2}$, $k_a = 3.00 \times 10^{-3}\ cm \cdot s^{-1}$, and $k_d = 1.10 \times 10^2\ s^{-1}$. For a 0.66 mm radius bubble in 1 mM 1-pentanol solution, the dimensionless distance x_e/R for reaching the equilibrium state can be estimated as $x_e/R \sim \rho g R \tau_e/(9\mu) = 6.25$. In both experiments and numerical simulations, domain sizes are large enough so that the interfacial surfactant concentration reaches the equilibrium state, and the bubble reaches steady-state velocity U_t before colliding on the free surface. Parameters corresponding to 5 mM 1-pentanol solution are listed in table I.

TABLE I. Parameters for 5 mM 1-pentanol solution

Temperature (Celsius)	2.1×10^1
Surface tension of pure water ($dyne/cm$)	7.2×10^1
Surface tension of 5 mM 1-pentanol ($dyne/cm$)	6.8×10^1
Maximum interfacial surfactant concentration Γ_∞ (mol/cm^2)	5.9×10^{-10}
Adsorption kinematic coefficient k_a (cm/s)	3.0×10^{-3}
Desorption kinematic coefficient k_d (s^{-1})	1.1×10^2
Bubble size R (mm)	6.6×10^{-1}

The list of dimensionless parameters is summarized in table II. The characteristic velocity of bubble $U = \rho g R^2/9\mu$ is used to evaluate dimensionless parameters. Note that there is no fitting parameter in the numerical simulations.

B. Numerical implementation

A front-tracking/finite-volume method [22, 23] is applied to solve Eqs. (2) and (4) on fixed uniform cartesian staggered grids. The time discretization is obtained using the first-order Euler method. Diffusion terms in Eqs. (2) and (4) are solved using central-difference schemes. In Eqs. (2) and (4), the convection terms are solved using QUICK (quadratic

TABLE II. Dimensionless parameters for 5 mM 1-pentanol solution

Reynolds number, $Re_U = 2\rho UR/\mu$	6.3×10^2
Capillary number, $Ca_U = \mu U/\sigma$	6.6×10^{-3}
Bulk Péclet number, $Pe = 2UR/D_c$	6.3×10^1
Interfacial Péclet number, $Pe_S = 2UR/D_S$	6.3×10^1
Density ratio, ρ_i/ρ_o	8.2×10^2
Viscosity ratio, μ_i/μ_o	5.5×10^2
Adsorption kinematics, $k = k_a C_\infty/k_d\Gamma_\infty$	2.3×10^{-1}
Biot number, $Bi = 2k_dR/U$	3.1×10^{-1}
Damkohler number, $Da = \Gamma_\infty/DC_\infty$	8.9×10^{-4}
Elasticity number, $\beta_S = RT\Gamma_\infty/\sigma$	2.0×10^{-1}

upstream interpolation for convective kinetics) [24] and upwind fifth order WENO-Z scheme [25], respectively. The projection method is utilized to enforce the continuity condition in Eq. (1), and resultant Poisson equation for the pressure is solved using the Hypre library [26]. Both bubble interface and free surface are represented by unstructured Lagrangian triangular grids. Eq. (5), which governs the evolution of interfacial surfactant concentration, is solved on these Lagrangian grids. On each triangular element Δ_e, Eq. (5) is written in an integral form,

$$\frac{d}{dt}\int_{\Delta_e} \Gamma dA = D_s \int_{\Delta_e} \nabla_s^2 \Gamma dA + \int_{\Delta_e} \dot{S}_\Gamma dA. \tag{8}$$

The term on the left hand side of Eq. (8) is solved using a first order explicit Euler method; the surface Laplacian term in Eq. (8) is solved in an identical way used for the calculation of curvature κ in Eq. (2). More details on the numerical implementation can be found in references [11, 22, 23].

In the simulation, a spherical bubble of radius R is initially placed at the center of $x-y$ plane and rises from location z_o, which is $2R$ away from the bottom. The size of the computational domain is $9R \times 9R \times 36R$ in x, y, and z directions, respectively. The free surface is located $3R$ away from the top of the computational domain. Flow field $\mathbf{u}$, pressure p, and surfactant bulk concentration C satisfy the periodic condition at side boundaries of the rectangular computational domain while both top and bottom boundaries satisfy no-slip wall boundary conditions.

IV. RESULTS AND DISCUSSION

A. Collision process in pure water and 1-pentanol solution

In Figure 2, experimental observations indicate that the presence of surfactant significantly modifies the collision process compared with pure water (also see Movie 1 [27]). Here we focus on the first collision of a 0.66 mm bubble with the free surface. In order to characterize the collision process, three distinct time instants are identified in Figure 2(b). T1, T2, and T3, respectively, correspond to the instants when the free surface starts affecting the bubble velocity ($U|_{\mathrm{T=T1}} = 0.95\ U_t$), when the bubble velocity becomes zero after colliding on the free surface, and when the bubble reaches a maximum velocity after reversing its direction of the motion. Therefore, the pre-collision stage is defined as the period of time from T1 to T2, and post-collision stage is from T2 to T3.

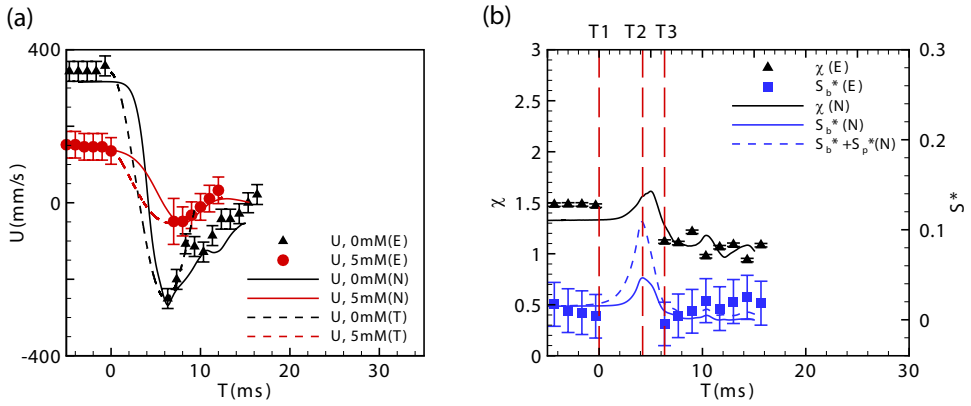

FIG. 2. (Color online)(a) Bubble's vertical velocity during the collision process for 0 mM and 5 mM 1-pentanol solutions obtained using (E) experimental, (N) numerical, and (T) theoretical studies. (b) In the pure water, the temporal evolution of bubble's deformation χ and dimensionless surface change S^* are recorded through numerical simulations and experiments. Error bars indicate the uncertainty of experimental measurements (see the Appendix). Bubble's size is $R = (6\mathscr{V}_b/\pi)^{1/3}/2 = 0.66\ mm$, where $\mathscr{V}_b$ is the bubble volume. In the theoretical model, the collision process is modeled as an under-damped mass spring system (see the Appendix).

A comparison of total energy transfer during the collision between pure water and surfactant solution can facilitate the interpretation of the collision dynamics. We compare the total energy transfer of the collision process. The instantaneous total energy consists of

surface energy due to the deformation of the bubble, surface energy due to the deformation of the free surface, and kinetic energy associated to the translation of the bubble. At time T1, the normalized total energy E^*_{T1} is written as

$$E^*_{\mathrm{T1}} = \frac{\Delta E|_{\mathrm{T=T1}}}{E_r} = \left(\frac{E_k}{E_r} + S^*_b + S^*_p\right)\Big|_{\mathrm{T=T1}}, \tag{9}$$

where $\Delta E = E - E_r$, E is the total energy of the bubble and free surface, $E_r = 4\pi\sigma R^2$ is the energy of a spherical bubble with the equivalent radius R at rest [13], $E_k = C_M(\chi)\rho\mathscr{V}_b U^2/2$ is the kinetic energy associated with the bubble motion, χ is the deformation of the bubble, and C_M is the added mass coefficient by assuming the bubble's shape as an oblate spheroid [28, 29],

$$C_M = \frac{(\chi^2-1)^{1/2} - \cos^{-1}\chi^{-1}}{\cos^{-1}\chi^{-1} - (\chi^2-1)^{1/2}\chi^{-2}}. \tag{10}$$

Changes in the surface area of the bubble interface and the free surface in dimensionless form are represented as $S^*_b = \Delta S_b/(4\pi R^2)$ and $S^*_p = \Delta S_p/(4\pi R^2)$, respectively. Even though the surface tension values for pure water and surfactant solution are comparable (72.2 $dyne/cm$ and 67.9 $dyne/cm$ measured at $T = 21°\mathrm{C}$, respectively), the estimated energy E^*_{T1} for water is about 7.45 times larger than that in the 5 mM 1-pentanol solution. This is due to the large bubble velocity in pure water ($Re = 2\rho U_t R/\mu = 438$) compared with that in 5 mM 1-pentanol solution ($Re = 195$), shown in Figure 2(a). At time T2, $E^*_{\mathrm{T2}} = \left(S^*_b + S^*_p\right)\big|_{\mathrm{T=T2}}$. During the pre-collision stage, the bubble kinetic energy is transfered to the surface energy of both bubble interface and free surface. The computation of $E^*_{\mathrm{T2}}/E^*_{\mathrm{T1}}$ is only available using the numerical simulations, and we find this ratio to be 88.7% for pure water and 74.4% for 5 mM 1-pentanol solution. The second phase of collision process corresponds to post-collision stage. From Figure 2, at time T3, the total surface change $\left(S^*_b + S^*_p\right)$ is close to zero, and kinetic energy associated to the bubble motion reaches its maximum.

During the entire bubble collision process, the total energy loss can be quantified by the coefficient of restitution, $\varepsilon = -U_{\mathrm{T3}}/U_{\mathrm{T1}}$. There is no energy loss when $\varepsilon = 1$. In the pure water experiment, the coefficient of restitution is 0.73. The large value of coefficient of restitution ($\varepsilon \geq 0.7$) indicates an elastic collision. However, in 5 mM 1-pentanol solution, we find this coefficient to be 0.32, and the bubble eventually detaches from the free surface. This reduced coefficient of restitution indicates a significant energy loss during the collision process, leading to a surfactant-induced partially inelastic collision.

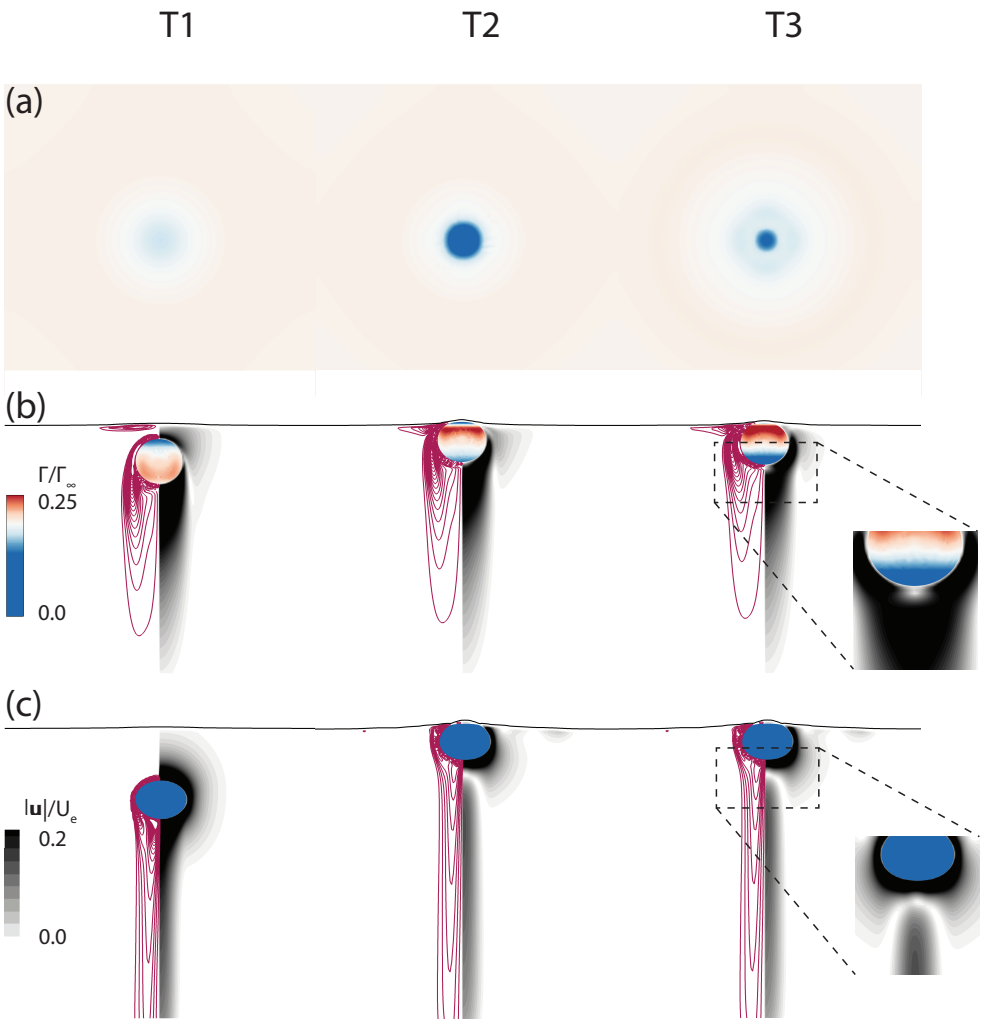

FIG. 3. (Color online) Colormaps show computational results for (a) interfacial surfactant concentration on the free surface, (b) velocity magnitude of the flow, and interfacial surfactant concentration on the bubble interface in 5 mM 1-pentanol solution, and (c) velocity magnitude of the pure water at time T1, T2, and T3. Contours of vorticity magnitude $|\boldsymbol{\Omega}|$ in (b) and (c) are shown at $0.05 : 0.05 : 1.0$. At time T3, the location of the stagnation points in both pure water and surfactant solution are visualized in insets. The bubble radius in both pure water and surfactant solution is 0.66 mm. The flow velocity in (b) and (c) is normalized by the bubble velocity in the Stoke flow, $U_e = \rho g R^2/(9\mu)$. The flow vorticity in (b) and (c) is normalized by $\Omega_e = U_e/R$.

The reduced rebound velocity in the surfactant solution can be explained by exploring the flow structure around a bubble in both pure water and 5 mM 1-pentanol solution during the collision process (see Movie 2 [27]). At time T1, a thin wake structure is formed in pure water due to the slip condition at the bubble interface (Figure 3(c)). However, the

bubble's wake in 5 mM 1-pentanol solution (Figure 3(b)) is distinct from that of a clean bubble. By visualizing the interfacial surfactant concentrations Γ on the bubble interface (see Figure 3(b) at T1), we observe that surfactant molecules migrate toward the rear side of the bubble, where Γ reaches its maximum. At the rear of the bubble, the local gradient of the interfacial tension leads to the Marangoni stress, immobilizing the bubble interface. Consequently, a distinct wake structure is formed in surfactant solution compared to that in the pure water. At time T2 when the bubble comes in contact with the free surface, both bubble and free surface show significant deformations in the pure water (see Figure 3(c)), where the morphology of free surface is represented by solid black lines. However, the deformations of both bubble and free surface are small in the presence of surfactant. At time T2, surfactants on the bubble interface (Figure 3(b)) start migrating away from the rear of the bubble, indicating a change of the direction of the interfacial convection on the bubble interface. In the meantime, surfactants on the free surface (Figure 3(a)) migrate away from the contact region. At time T3, the locations of the stagnation points ($|\mathbf{u}| = 0$ in the wake region) for pure water and surfactant solution are different. In the surfactant solution, the stagnation point is at the bubble interface, and the bubble has a small coefficient of restitution. However, the stagnation point is further away from the bubble interface for the pure water, and the bubble exhibits large coefficient of restitution.

The small coefficient of restitution in surfactant solution can be explained by the generation of the vorticity ($\mathbf{\Omega} = \nabla \times \mathbf{u}$) during the collision process. In the surfactant solution, the vorticity is generated at the free surface before the bubble approaches the free surface (see Figure 3(b)). As the bubble rises towards the free surface, the associated fluid flow creates non-uniform spatial distribution of interfacial surfactant concentration along the free surface. The non-uniform distribution of surfactant molecules creates Marangoni stresses leading to the generation of additional vorticity near the free surface (Figure 3(b)), which is absent in the pure water (Figure 3(c)). The vortical structure near the free surface persists during the entire collision process (see Figure 3). Following the work of Stone [30], who expressed the viscous energy dissipation rate in terms of vorticity field, we have $\frac{2}{\pi Re}\int_V \phi dV = \frac{2}{\pi Re}\int_V \mathbf{\Omega}^2 dV + \frac{4}{\pi Re}\int_S \kappa U_s^2 dS$, where ϕ is the viscous energy dissipation rate; V and S represent the fluid domain and bubble surface, respectively. Therefore, the occurrence of additional vorticity near the free surface in the surfactant solution enhances the viscous dissipation rate and leads to a reduced coefficient of restitution.

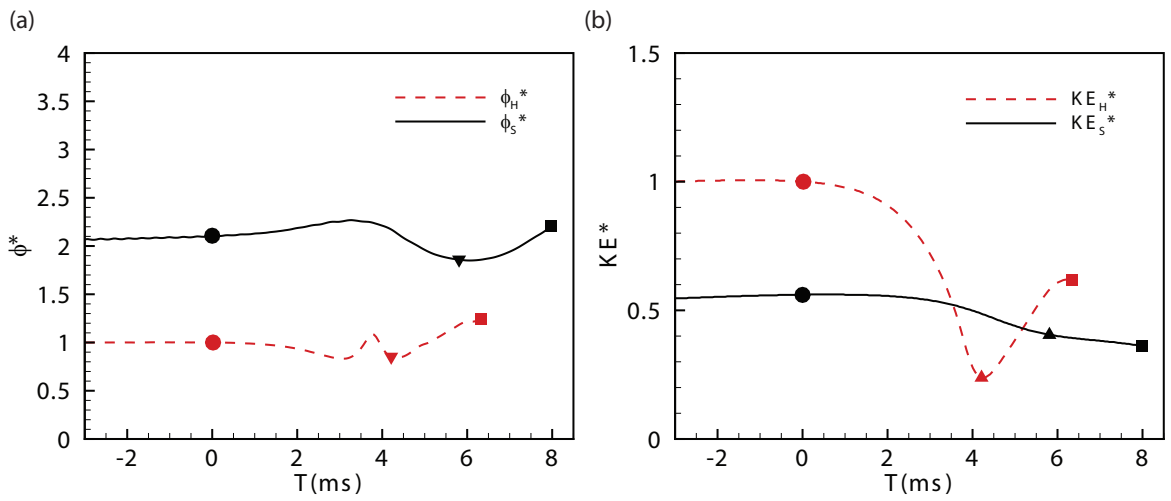

FIG. 4. (Color online) The evolution of (a) viscous dissipation rate and (b) kinetic energy are recorded during the collision process in both 0 mM and 5 mM 1-pentanol solutions, corresponding to subscripts H and S, respectively. Solid circle, triangle, and square symbols indicate times T1, T2, and T3, respectively.

Here, we quantify the temporal evolution of viscous dissipation rate ($\phi = \int 2\mu \boldsymbol{E} : \boldsymbol{E} dV$) and kinetic energy ($KE = \int \frac{1}{2}\rho \boldsymbol{u}^2 dV$) from our computational results, where $\boldsymbol{E}$ is the strain rate tensor. In Figure 4(a), the normalized viscous dissipation rate is defined as $\phi^* = \phi/\phi_H^{\mathrm{T1}}$, where ϕ_H^{T1} is the viscous dissipation rate in pure water at time T1. The viscous dissipation rate in pure water decreases in the beginning of collision process. On the other hand, the viscous dissipation rate in the surfactant solution increases. Although the bubble's velocity decreases in the presence of surfactant, the additional vortical structure induced by the Marangoni stress at the free surface (see Figure 3(b)) enhances the overall viscous dissipation rate. The kinetic energy in the entire domain is shown in Figure 4(b), where $KE^* = KE/KE_H^{\mathrm{T1}}$ is the normalized kinetic energy. The kinetic energy in pure water increases after collision, which is associated with the bubble's bouncing motion. On the other hand, the kinetic energy in the surfactant solution monotonically decreases during the collision process. To sum up, the enhanced viscous dissipation rate during the collision process in the surfactant solution compared to that in pure water leads to reduction of the coefficient of restitution.

B. Effect of surfactant concentration

Depending on surfactant concentration, bubble's collisions exhibit elastic, partially inelastic, and perfectly elastic behaviors. We first categorize the collision process using a phase diagram. Next, we examine the effect of surfactant concentration on the drag acting on the bubble and the coefficient of restitution. In addition, the dynamics of the collision process in surfactant solution is compared with rigid particles colliding on a rigid wall.

In the pure water, the bubble's collision behavior on a free surface is dominated by the viscous drainage process [14–17], and our results follow $\varepsilon_H = \exp(-17\sqrt{Ca/St})$ (see the Appendix), where $Ca = U_t\mu/\sigma$ and $St = 2\rho C_M R U_t/(9\mu)$ [29]. The Capillary number Ca represents the ratio of the viscous force to the surface tension, and Stokes number St characterizes the relative effect of inertial force associated with the bubble's added mass to the viscous drag. For surfactant solutions, both mean interfacial surfactant concentration and surface tension solely depend on Langmuir number La at the equilibrium state. Langmuir number, $La = \frac{k_a C_\infty}{k_d \Gamma_\infty}$, is defined as the ratio between the surfactant adsorption and desorption rates happening on the gas-liquid interfaces. For a given β, $\Gamma_o/\Gamma_\infty = 1/(1 + La^{-1})$ and $\sigma/\sigma_0 = 1 - \beta \ln(1 + La)$. Therefore, large La results in a high interfacial surfactant concentration, reducing the surface tension force and modifying the Marangoni stress. In this work, we use La to characterize the extent of Marangoni stress. In Figure 5(b), we quantify the coefficient of restitution in terms of La and Ca/St, where La and Ca/St characterize the extent of Marangoni stress and viscous drainage, respectively. When there are strong Marangoni and viscous effects ($La > 0.5$ and $Ca/St > 2 \times 10^{-4}$), bubbles remain attached to the free surface, exhibiting perfectly inelastic collisions. The collisions are elastic when $La \sim 0$ and $Ca/St < 1 \times 10^{-4}$.

The drag acting on the bubble prior to the collision is influenced by surfactant concentration. The drag coefficient is defined as $C_D = 2F/\left(\rho U_t^2 \pi R^2\right)$, where F is the drag acting on the bubble. The modified drag due to surfactants can be written as $C_D/C_{D,H}$, where $C_{D,H}$ is the drag acting on a bubble in pure liquids, $C_{D,H} = 48\left(G(\chi)/Re\right)\left(1 + H(\chi)/Re^{1/2}\right)$ and coefficients G and H are given in the article by Moore [31]. Surfactants enhance the drag compared to pure water ($C_D/C_{D,H} - 1 > 0$, and see Figure 5(a)). The extent of drag enhancement depends on the value of La: $C_D/C_{D,H}$ increases at low La and decreases at large La. At small La, the enhanced drag is scaled as $C_D/C_{D,H} - 1 \propto La^2$, which is consistent

with the theory in Stokes regime [32]. At large La ($1 < La < 10$), we find it to scale as $C_D/C_{D,H} - 1 \propto La^{-0.37}$, and similar trend has been found in the numerical study of Wang *et al.* [5] at zero Reynolds number .

A normalized coefficient of restitution can be defined as $\varepsilon/\varepsilon_H$ to eliminate the contribution from the viscous drainage. From Figure 5(a), surfactants reduce the coefficient of restitution ($\varepsilon/\varepsilon_H < 1$). The effect of surfactant on $\varepsilon/\varepsilon_H$ is non-monotonic (Figure 5(a)), and its maximum reduction occurs at $La \sim 1$. In the limit of small La, $\varepsilon/\varepsilon_H \sim \exp(-5La)$; at large La, $\varepsilon/\varepsilon_H$ increases with La as $\varepsilon/\varepsilon_H \propto La^{0.2}$.

For both bubble's drag and its coefficient of restitution, the maximum effect of surfactact happens when $La \sim O(1)$, which can be explained by the following scaling analysis. The magnitude of Marangoni stress is estimated as $|\nabla\sigma|$ [5]. During the equilibrium state, $\dot{S}_\Gamma = 0$ in Eq. (6), and we get

$$\nabla\sigma = \frac{\sigma_0\beta}{\Gamma/\Gamma_\infty - 1}\frac{La}{(1 + La \cdot C/C_\infty)^2}\nabla\left(\frac{C}{C_\infty}\right). \tag{11}$$

From Eqs. (5) and (7), a balance between the convection and mass source terms provides that $|\nabla C| \sim \frac{\Gamma_o U_t}{D_C R}$, where $\Gamma_o = \frac{La}{1+La}\Gamma_\infty$. The Marangoni stress normalized by the viscous stress is estimated as $|\nabla_S\sigma|/(\mu U_t/a) \sim \frac{\sigma_0\beta k_a}{D_C\mu k_d} \cdot \frac{La}{(1+La)^2}$. Therefore, the scaling analysis suggests that surfactants have a larger contribution to the collision process compared to the viscous drainage when $La = 1$.

In Figure 5(c), our experimental data is compared against previously reported experimental data in the pure liquids [14–16] as well as the limit of solid particles colliding on a rigid wall [33, 34]. At large Stokes number ($St \sim O(100)$) where there is a low surfactant concentration (Low La, see Figure 5(d)), the bubble's collision behavior is close to the clean one. This clean limit can be characterized by $\varepsilon = \exp(-1.8St^{-1/2})$ [29]. However, the coefficient of restitution deviates from this clean limit as St decreases. When $St < 10$, surfactant immobilizes both the bubble interface and free surface, and our data resembles a rigid particle colliding onto a rigid wall; this behavior can be well predicted by the elasto-hydrodynamics theory [34]. The collision behavior between these two limits is governed by the Marangoni stresses, and the Langmuir number can be used to describe the coefficient of restitution.

Finally, we quantify the temporal evolution of viscous dissipation rate in the entire computational domain for different concentrations of 1-pentanol solution from our numerical

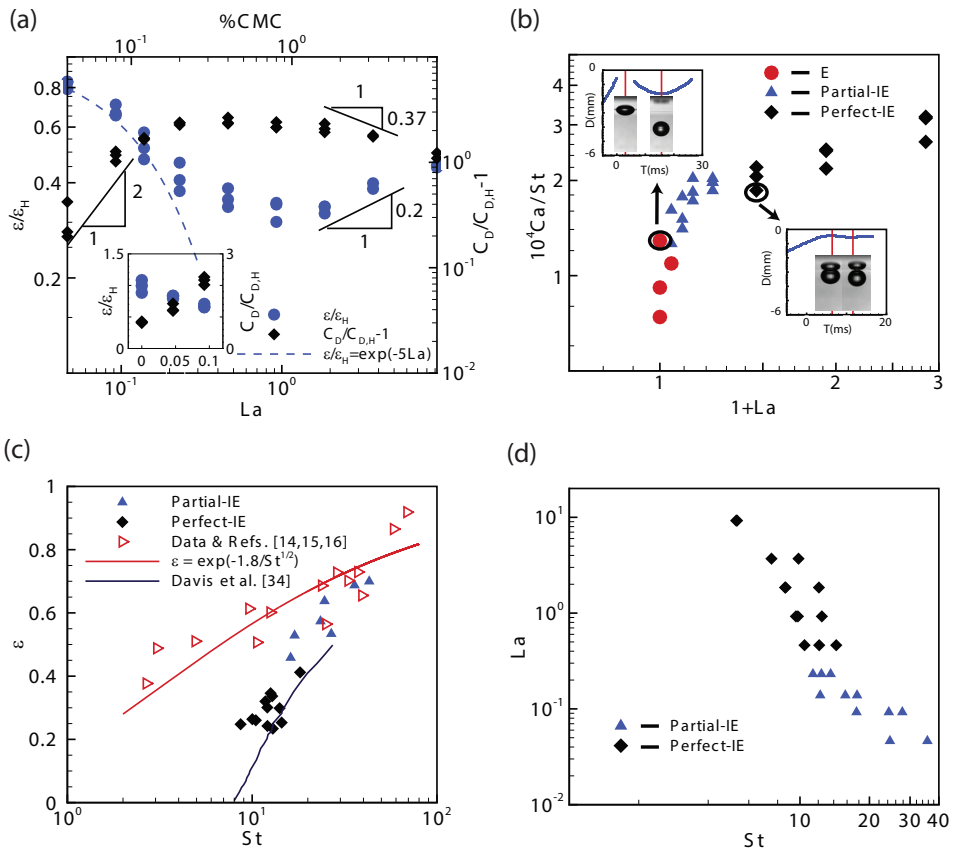

FIG. 5. (Color online)(a) Normalized coefficient of restitution and drag coefficient are plotted as a function of La number. (b) The phase diagram depicts bubble behavior ranging from elastic (E) to inelastic (Partial-IE) to perfectly inelastic (Perfect-IE) collision, shown in terms of La and Ca/St. (c) The coefficient of restitution is plotted as a function of St number. (d) The effect of surfactant concentration (La) on the bubble's St number.

results (see Figure 6(a)). The ratio of viscous dissipation rate between time T3 and T1 as a function of Langmuir number in Figure 6(b) follows a similar trend as the coefficient of restitution.

V. CONCLUSION

Collisions between bubbles and a free surface are frequently observed in aquatic environments, and surfactants effectively modify relevant dynamics compared with that in the pure water. In this study, we examine the Marangoni effect in the context of a dynamic interfacial problem through both experiments and numerical simulations. In surfactant solutions, we

find that the Marangoni stress induces additional vorticity near the free surface, causing extra dissipation and consequently reducing the rebound velocity. The Marangoni effect, characterized by Langmuir number, enhances the bubble's drag and reduces the coefficient of restitution. Their dependence on the surfactant concentration is non-monotonic. The maximum enhancement of the drag and reduction of the coefficient of restitution occur at $La \sim O(1)$.

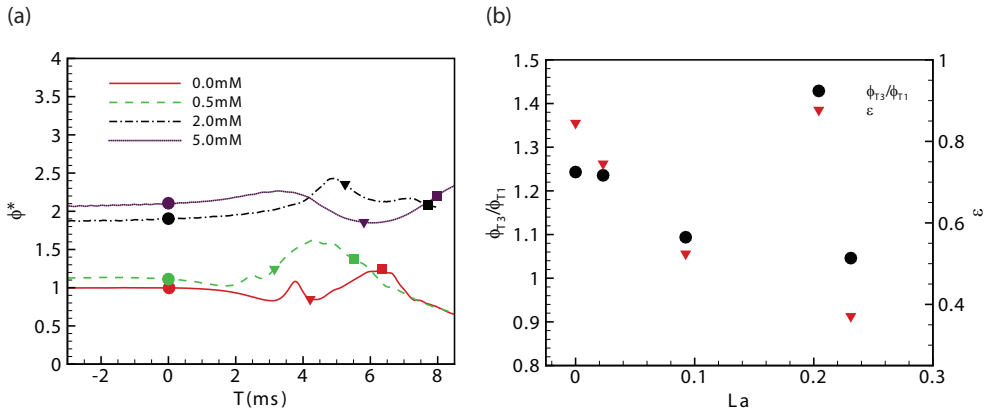

FIG. 6. (Color online)(a) The evolution of viscous dissipation rate is recorded during the collision process for different concentrations of 1-pentanol solutions, where solid circle, triangle, and square symbols indicate times T1, T2, and T3, respectively. (b) The ratio of viscous dissipation rate between time T3 and T1, and coefficient of restitution are plotted as a function of La number. For both (a) and (b), bubble radius is $R = 0.66\ mm$.

ACKNOWLEDGMENTS

We thank J. W. M. Bush for fruitful discussions. This work was partially supported by a grant from Pioneer Oil Company.

Appendix A: Surface tension measurements for 1-pentanol solution

Surface tension for aqueous solution of 1-pentanol at 21°C is measured as a function of concentration. Figure 7 compares our measured data to the empirical relationship provided in the literature [21]. This empirical relationship is described by the Szyszkowski equation,

$$\sigma = \sigma_0 - \frac{\mathscr{R}T}{\omega} \ln(1 + kC), \tag{A1}$$

where $\omega = 1.48 \times 10^5\ m^2/mol$ and $k = 66\ dm^3/mol$ [21].

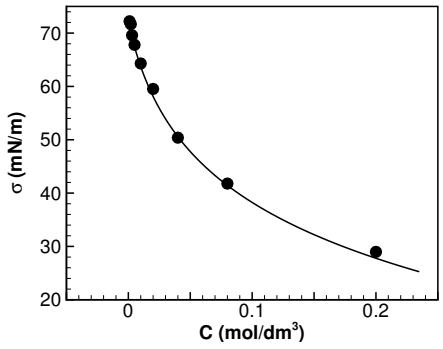

FIG. 7. Measured surface tensions for 1-pentanol solution (black solid circles); solid line is Szyszkowski equation [21].

Appendix B: Uncertainty quantification for experiments

There are two major uncertainty sources in the experimental post-processing procedure. They are the uncertainties of the calibration process, and the variation in the pre-selected threshold for bubble image binarization. After calculating each uncertainty, the total uncertainty is synthesized by the Taylor series approximation of the elemental uncertainties. The uncertainty of the calibration process is straightforward, and here, we report the methodology for uncertainty due to pre-selected threshold.

The variation of the threshold during image binarization affects the detected bubble profile and shape, which leads to uncertainty in the estimation of bubble's center, radius, deformation, surface area, volume, and other derived quantities. This uncertainty is quantified by examining the r.m.s. of the reported parameters by continuously changing the threshold values.

Appendix C: Under-damped mass spring system

The dynamics of bubble's collision process are modeled as an under-damped mass spring system (see Figure 8(a))

$$m\frac{d^2\eta}{dt} + \mathscr{C}_{\mu,C}\frac{d\eta}{dt} + \mathscr{C}_{\sigma}\eta = 0, \tag{C1}$$

where $m = \frac{4}{3}\pi R^3 \rho C_M$ is the added mass of the bubble, $\mathscr{C}_{\mu,C}$ characterizes the drag during the collision process in a surfactant solution, and $\mathscr{C}_\sigma = K_1K_2/(K_1+K_2) = k_1k_2\sigma/(k_1+k_2) = \mathscr{K}\sigma$. Rewriting Eq. (C1) gives

$$\frac{d^2\eta}{dt} + 2\xi(St, Ca, La)\omega\frac{d\eta}{dt} + \omega^2\eta = 0, \tag{C2}$$

where $\xi = \mathscr{C}_{\mu,C}/(2m\omega)$ is the damping ratio, and $\omega = \sqrt{\mathscr{K}\sigma/m}$ is the natural frequency. A reduced bouncing velocity occurs due to the viscous drag (low St) and Marangoni stress (large La). During the collision process, the normalized bubble velocity is expressed as

$$U/U_t = \dot{\eta}(t)/U_t = e^{-\xi\omega t}\cos\left(\omega t\sqrt{1-\xi^2}\right). \tag{C3}$$

In our experiments, the coefficient of restitution and natural frequency are calculated as $\varepsilon = -U_{\mathrm{T3}}/U_{\mathrm{T1}} = e^{-\xi\pi/\sqrt{1-\xi^2}}$ and $\omega_o = \pi\left(1-\xi^2\right)^{-1/2}/\left(\mathrm{T3}-\mathrm{T1}\right)$, respectively.

In a pure fluid, $\mathscr{C}_{\mu,C} = \mathscr{C}_\mu = a\mu R$ [29], where a is a constant. Therefore, the damping ratio can be written as $\xi = \frac{a}{\sqrt{24\pi\mathscr{K}}}\sqrt{\frac{Ca}{St}}$. Since $\frac{Ca}{St} \sim O(10^{-4})$, $\varepsilon \sim e^{-\mathscr{M}\sqrt{\frac{Ca}{St}}}$ in the case of $\xi \ll 1$, where $\mathscr{M}$ is a fitting parameter. By combining data from our experiments and literature [14–16], we find that $\mathscr{M} = 17$ provides the best fit (see Figure 8(b)).

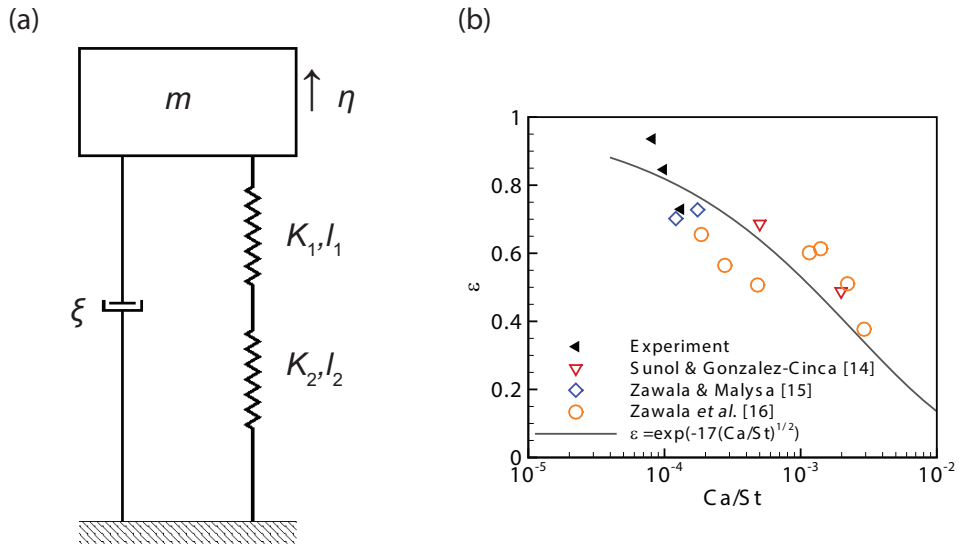

FIG. 8. (Color online) (a)Mass-spring-damper model: two springs are connected in series; the dashpot and springs are connected in parallel. K_1 and K_2 are the spring stiffness of free surface and bubble, respectively; natural length l_1 corresponds to an undeformed free surface while l_2 incorporates the initial deformation of the rising bubble; m is the added mass of the bubble; ξ is the damping ratio, which incorporates the contribution to the drag from both the viscous force and Marangoni stress. (b) The derived relationship between coefficient of restitution ε and Ca/St is provided based on data from our experiments and literature.

[1] R. B. Fdhila and P. C. Duineveld, The effect of surfactant on the rise of a spherical bubble at high reynolds and peclet numbers, Phys. Fluids **8**, 310–321 (1996).

[2] S. Takagi and Y. Matsumoto, Surfactant effects on bubble motion and bubbly flows, Annu. Rev. Fluid Mech. **43**, 615–636 (2011).

[3] A. Frumkin and V. G. Levich, On surfactants and interfacial motion, Zh. Fiz. Khim. **21**, 1183–1204 (In Russian) (1947).

[4] B. Cuenot, J. Magnaudet, and B. Spennato, The effects of slightly soluble surfactants on the flow around a spherical bubble, J. Fluid Mech. **339**, 25–53 (1997).

[5] Y. Wang, D. T. Papageorgiou, and C. Maldarelli, Increased mobility of a surfactant-retarded bubble at high bulk concentrations, J. Fluid Mech. **390**, 251–270 (1999).

[6] M. Fukuta, S. Takagi, and Y. Matsumoto, Numerical study on the shear-induced lift force acting on a spherical bubble in aqueous surfactant solutions, Phys. Fluids **20**, 040704 (2008).

[7] Y. Zhang and J. A. Finch, A note on single bubble motion in surfactant solutions, J. Fluid Mech. **429**, 63–66 (2001).

[8] Y. Tagawa, S. Takagi, and Y. Matsumoto, Surfactant effect on path instability of a rising bubble, J. Fluid Mech. **738**, 124–142 (2014).

[9] M. Muradoglu and G. Tryggvason, A front-tracking method for computation of interfacial flows with soluble surfactants, J. Comput. Phys. **227**, 2238–2262 (2008).

[10] S. Tasoglu, U. Demirci, and M. Muradoglu, The effect of soluble surfactant on the transient motion of a buoyancy-driven bubble, Phys. Fluids **20**, 040805 (2008).

[11] M. Muradoglu and G. Tryggvason, Simulations of soluble surfactants in 3d multiphase flow, J. Comput. Phys. **274**, 737–757 (2014).

[12] L. Doubliez, The drainage and rupture of a non-foaming liquid film formed upon bubble impact with a free surface, Int. J. Multiphase Flow **17**, 783–803 (1991).

[13] H. K. Tsao and D. L. Koch, Observations of high reynolds number bubbles interacting with a rigid wall, Phys. Fluids **9**, 44–56 (1997).

[14] F. Suñol and R. González-Cinca, Rise, bouncing and coalescence of bubbles impacting at a free surface, Colloids Surf., A **365**, 36–42 (2010).

[15] J. Zawala and K. Malysa, Influence of the impact velocity and size of the film formed on

bubble coalescence time at water surface, Langmuir **27**, 2250–2257 (2011).

[16] J. Zawala, S. Dorbolo, D. Terwagne, N. Vandewalle, and K. Malysa, Bouncing bubble on a liquid/gas interface resting or vibrating, Soft Matter **7**, 6719–6726 (2011).

[17] R. Manica, E. Klaseboer, and D. Y. C. Chan, The impact and bounce of air bubbles at a flat fluid interface, Soft Matter **12**, 3271–3282 (2016).

[18] T. S. Light, S. Licht, A. C. Bevilacqua, and K. R. Morash, The fundamental conductivity and resistivity of water, Electrochem. Solid-State Lett. **8**, E16–E19 (2005).

[19] S. Takagi, T. Uda, Y. Watanabe, and Y. Matsumoto, Behavior of a rising bubble in water with surfactant dissolution (1st report, steady behavior), Trans. JSME B **69**, 2192–2199 (2003).

[20] V. B. Fainerman and S. V. Lylyk, Dynamic surface-tension and kinetics of adsorption in solutions of normal alcohols, Colloid J. **44**, 538–544 (1982).

[21] M. J. Hey and P. G. Kippax, Surface tensions of mixed aqueous solutions of tert-butanol and n-pentanol, Colloids Surf., A **262**, 198–203 (2005).

[22] S. Dabiri, A. Doostmohammadi, M. Bayareh, and A. M. Ardekani, Rising motion of a swarm of drops in a linearly stratified fluid, Int. J. Multiphase Flow **69**, 8–17 (2015).

[23] S. Dabiri and G. Tryggvason, Heat transfer in turbulent bubbly flow in vertical channels, Chem. Eng. Sci. **122**, 106–113 (2015).

[24] B. P. Leonard, A stable and accurate convective modelling procedure based on quadratic upstream interpolation, Comput. Method Appl. M. **19**, 59–98 (1979).

[25] R. Borges, M. Carmona, B. Costa, and W. S. Don, An improved weighted essentially non-oscillatory scheme for hyperbolic conservation laws, J. Comput. Phys. **227**, 3191–3211 (2008).

[26] R. Falgout and U. Yang, Hypre: A library of high performance preconditioners, Computational Science - ICCS **2331**, 632–641 (2002).

[27] See Supplemental Material at (DOI) for two movies. Moive 1 shows temporal evolution of both vertical position of bubble center and bubble's translational velocity in both pure water and 5 mM 1-pentanol solution. Bubble's collision process in the 5 mM 1-pentanol solution via numerical simulation is shown in Movie 2.

[28] H. Lamb, *Hydrodynamics* (Cambridge University Press, Cambridge, 1932).

[29] R. Zenit and D. Legendre, The coefficient of restitution for air bubbles colliding against solid walls in viscous liquids, Phys. Fluids **21**, 083306 (2009).

[30] H. A. Stone, An interpretation of the translation of drops and bubbles at high reynolds num-

bers in terms of the vorticity field, Phys. Fluids **5**, 2567–2569 (1993).

[31] D. W. Moore, The velocity of rise of distorted gas bubbles in a liquid of small viscosity, J. Fluid Mech. **23**, 749–766 (1965).

[32] L. G. Leal, *Advanced transport phenomena: fluid mechanics and convective transport processes* (Cambridge University Press, Cambridge, 2007).

[33] G. G. Joseph, R. Zenit, M. L. Hunt, and A. M. Rosenwinkel, Particle–wall collisions in a viscous fluid, J. Fluid Mech. **433**, 329–346 (2001).

[34] R. H. Davis, J. M. Serayssol, and E. J. Hinch, The elastohydrodynamic collision of two spheres, J. Fluid Mech. **163**, 479–497 (1986).